

CUP BURNER FLAME EXTINGUISHMENT BY BROMINATED COMPOUNDS

Gregory T. Linteris
Fire Research Division, National Institute of Standards and Technology
Gaithersburg, MD 20899 USA
Tel: 301-975-2283; Fax: 301-975-4052; linteris@nist.gov

Fumiaki Takahashi
National Center for Space Exploration Research on Fluids and Combustion
NASA Glenn Research Center
21000 Brookpark Road
Cleveland, OH 44135
Tel: 216-433-3778; Fax: 216-433-3793; Fumiaki.Takahashi@grc.nasa.gov

and

Viswanath R. Katta
Innovative Scientific Solutions, Inc.
2766 Indian Ripple Road
Dayton, OH 45440
Tel: 937-255-8781; Fax: 937-255-3139; vrkatta@innssi.com

ABSTRACT

Experiments and calculations have been performed for a methane-air cup-burner flame with added CF_3Br or Br_2 . The time-dependent, two-dimensional numerical code, which includes a detailed kinetic model and diffusive transport, has predicted the flame extinction within 4 % or 8 % for each. Analysis of the flame structure has allowed the mechanisms of flame weakening in the base and trailing flame regions to be compared. The agents CF_3Br and Br_2 behave very similarly with regard to flame extinguishment: both raise the temperature in the flame everywhere, as well as lower radical volume fractions in the trailing diffusion flame or the reaction kernel. The mechanism of lowered radical volume fractions is shown to be primarily due to a catalytic cycle involving bromine species in both regions of the flame, with small contributions from radical trapping by fluorinated species in the trailing diffusion flame. In the trailing diffusion flame, the effectiveness of the agents is reduced because the hydrocarbon species, which are necessary for the regeneration of HBr , are scarce at the location of the peak radical volume fraction (i.e., at the flame zone).

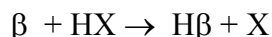
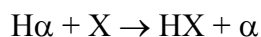
1.0 INTRODUCTION

The fire extinguishing agent trifluorobromomethane (CF_3Br , Halon 1301) is effective [1] and widely used [2]. Unfortunately, because of its destruction of stratospheric ozone, its production in industrialized nations has been banned [3]. Much recent research has been aimed at finding both short- [4, 5] and long-term [6] replacements for CF_3Br . As a result, CF_3Br itself has been the continuing subject of many studies [7-13] since an improved understanding of its mechanism

of inhibition will help in the search for alternatives, and nearly all assessments of new agents use CF₃Br as a baseline for comparison of the new agents.

The burner selected here is the so-called cup burner [14, 15], which is essentially a co-flow diffusion flame burner with a wide, low velocity fuel nozzle rather than the jet nozzle of typical co-flow diffusion flames. The cup burner is widely used in the fire protection industry as a scale model flame for testing total-flooding fire suppressants and is the basis of National Fire Protection Association (NFPA) [16] and ISO [17] standards. Typically, the agent is added to the co-flowing oxidizer stream and the minimum extinguishing concentration (MEC) is recorded. A vast database exists for the MEC of various fire suppressants with specific fuels (both liquid and gaseous), and these data provide the basis for the minimum design concentration for a particular agent to be used as a fire suppressant. While important research has been done with CF₃Br in cup-burner flames [18-20], the present work goes beyond the previous by providing some new measured parameters (including new data for Br₂ addition) and applying detailed numerical modeling to understand the flow-field and chemical kinetics important for CF₃Br or Br₂ extinguishment of cup-burner flames.

The basic mechanism of halogen flame inhibition was suggested by Rosser et al. [21] and further justified and refined by Butlin and Simmons [22], Dixon-Lewis and co-workers [23, 24], Westbrook [25-27], and Babushok and co-workers [28]. The reaction mechanism is:



in which X is a halogen, α is a hydrocarbon, and β is a reactive radical such as H, O, or OH. Hydrogen atom is typically affected most by the catalytic radical recombination cycles above, and its decrease leads to a lowering of the chain-branching reaction $H + O_2 \rightarrow OH + O$ and the CO consumption reaction $CO + OH \rightarrow CO_2 + H$. While it is generally believed that the same chemical mechanism is at work in the extinguishment of co-flow diffusion flames with added Br compounds, there have been no papers which describe the actual mechanism.

In recent years, numerical investigations [29-31] using detailed chemistry models have revealed the flame structure, blowoff phenomena, and physical and chemical suppression processes for co-flow jet diffusion flames. Major findings indicate that the blow-off process is controlled by behavior at the peak reactivity spot (i.e., reaction kernel), formed at the flame attachment point in the edge (base) of diffusion flames. More recently, the extinguishment of cup-burner flames with added inert agents [32] and CF₃H [33] has been studied. Nonetheless, most of the previous work has been with jet flames, and no cup-burner studies have yet been performed for brominated agents.

The overall objectives of the present study are to understand the physical and chemical processes of cup-burner flame suppression by CF₃Br and Br₂ and to provide rigorous testing of the numerical model, which includes detailed chemistry and radiation sub-models. This paper describes the experimental and numerical extinguishment limits, as well as the flame structure changes which occur near the limits, for methane as the fuel and CF₃Br or Br₂ as the agent.

2.0 EXPERIMENT

The burner [15, 34], consisted of a cylindrical glass cup (28 mm diameter) positioned inside a glass chimney (53.3 cm tall, 9.5 cm diameter). To provide uniform flow, 6 mm glass beads filled the base of the chimney, and 3 mm glass beads (with two 15.8 mesh/cm screens on top) filled the fuel cup (for gaseous fuels only). Calibrated mass flow controllers (Sierra 860¹) provided the gas flow with an uncertainty of 2 % of indicated flow. The flow rate of the co-flowing gas was held constant at 41.6 ± 0.8 L/min, and the CF₃Br or Br₂ was added to that flow. For bromine as the inhibitor, all flow tubes downstream of agent addition as well as the burner base were made of Teflon to avoid reaction. A computer-controlled syringe pump added the liquid Br₂ to a 2.1 m long tubing carrying the air, and complete Br₂ evaporation was observed to occur within a tubing length of less than 1 m. For determining the extinguishment condition, the agent was added to the flow (in increments of < 1 % near extinguishment), and the total flow increased slightly, until lift-off was observed. (For the present flow conditions, the MEC is relatively insensitive to the total flow [33].) The test is repeated at least three times. The co-flow oxidizer stream velocity U_{ox} with and without agent was 10.7 ± 0.21 cm/s, and the fuel jet velocity U_f was 0.921 ± 0.018 cm/s.

The fuel was methane (Matheson UHP, 99.9 %), and the air was house compressed air (filtered and dried) which was additionally cleaned by passing it through an 0.01 μm filter, a carbon filter, and a desiccant bed to remove small aerosols, organic vapors, and water vapor. The agents were Br₂ (Aldrich, 99.5 %) and CF₃Br (Great Lakes).

The flame images for the tests were recorded with video cameras and subsequently digitized. For CF₃Br addition, flame images were captured with a black and white Charge Coupled Device (CCD) video camera (Sony, XC-ST50), and an interference filter (Oriel No. 59295, 430 nm, bandwidth 10 nm) helped to resolve against soot emission and image CH in the reaction zone [35]. A video frame-grabber board (with a resolution of 640 x 480 and a framing rate of 2 Hz) in a Pentium-II based personal computer digitized the images, which were then analyzed to determine the flame base location using the NASA image processing freeware program Spotlight [36]. Thirty images were collected and subsequently analyzed for each flow condition of the flame. Note that in figures which follow, if the uncertainty is shown on the data points, the error bars represent the standard deviation (66 % confidence level) for the variation in the flame location for the 30 frames of data (caused by naturally occurring flame flicker).

For the measured parameters, an uncertainty analysis was performed, consisting of calculation of individual uncertainty components and root mean square summation of components. All uncertainties are reported as *expanded uncertainties*: $X \pm ku_c$, from a combined standard uncertainty (estimated standard deviation) u_c , and a coverage factor $k = 2$. Likewise, when

¹ Certain commercial equipment, instruments, or materials are identified in this paper for adequately specifying the procedure. Such identification does not imply recommendation or endorsement by NIST, nor does it imply that the materials or equipment are necessarily the best available for the intended use.

reported, the relative uncertainty is ku_c / X . The expanded relative uncertainties for the extinguishment volume fraction of CF_3Br and Br_2 are 2.7 % and 2.0 %.

3.0 NUMERICAL MODEL

The unsteady co-flow diffusion flames of the cup burner were simulated using a time-dependent, axisymmetric mathematical model known as UNICORN (UNsteady Ignition and COMbustion using ReactionNs) [37]. This model solves u- and v-momentum equations, continuity equation, and enthalpy- and species-conservation equations on a staggered-grid system. The body-force term due to the gravitational field is included in the axial-momentum equation to simulate vertically mounted flames in normal gravity. A clustered mesh system traces the gradients in flow variables near the flame surface. Calculations are made on a physical domain of 200 mm and 47.5 mm in the axial (z) and radial (r) directions, with a non-uniform grid system of 251×101 or 480×384 , constructed so that the minimum grid spacing in the flame zone is ≈ 0.2 mm or 0.08 mm, respectively, in both the z and r directions. The computational domain is confined by the axis of symmetry and wall boundaries in the radial direction and by the inflow and outflow boundaries in the axial direction. The outer boundary in the z direction is located sufficiently far from the burner exit (~ 15 fuel-cup radii) so that propagation of boundary-induced disturbances into the region of interest is minimal. Flat velocity profiles are imposed at the fuel and air inflow boundaries, while an extrapolation procedure with weighted zero- and first-order terms is used to estimate the flow variables at the outflow boundary. For accurate simulation of the flow structure at the base of the flame, which is very important in flame-extinguishment studies, the fuel-cup wall was treated as a 1-mm-long, 1-mm-thick tube in the calculations. For simulating the heat transfer between the burner rim and the flame, the temperature of the tubular rim was set at 600 K, which is somewhat higher than the $514 \text{ K} \pm 10 \text{ K}$ measured previously in the experiments. Since the flames at extinguishment are well lifted from the burner rim, heat losses to the rim, and hence the rim surface temperature, is not as crucial as it would be if our interest were primarily in the flame structure under the normal, stably attached condition.

The chemical kinetics of the CF_3Br -or Br_2 -inhibited cup-burner flames are described using a detailed chemical kinetic mechanism having 92 species and 1644 elementary-reaction steps, developed by the National Institute of Standards and Technology (NIST) [38] through addition of bromine- and fluorine-species inhibition reactions to the GRI-V1.2 combustion mechanism [39]. The thermo-physical properties such as enthalpy, viscosity, thermal conductivity, and binary molecular diffusion are calculated for each species from the polynomial curve fits developed for the temperature range 300 K to 5000 K. Mixture viscosity and thermal conductivity are then estimated using the Wilke and Kee expressions, respectively. Molecular diffusion is assumed to be of the binary-diffusion type, and the diffusion velocity of a species is calculated using Fick's law and the effective-diffusion coefficient of that species in the mixture. A simple radiation model based on the optically thin-media assumption [40] was incorporated into the energy equation. Only radiation from CO_2 , H_2O , CO , and CH_4 was considered in the present study.

4.0 RESULTS AND DISCUSSION

4.1. FLAME EXTINGUISHMENT RESULTS

The experimental and numerical results (and the discrepancy between the two) for cup-burner flames of methane and air extinguished by pure CF_3Br or Br_2 are indicated in Table 1. The numerical code predicts the MEC for CF_3Br to be $(2.49 \pm 0.01) \%$, or about 4 % higher than the experiment (the uncertainty in the numerical prediction reported here is the change in CF_3Br volume fraction between simulations which caused, or did not cause, flame extinguishment), while the prediction for Br_2 is 0.0167, or about 8 % higher than the experiment. Similar good predictive ability has been found for, CF_3H , CO_2 , He, N_2 , and Ar [41], which are also shown in the table (in order of decreasing effectiveness)[33, 42]. These close results (generally within about 8 %) for all of the simulations with the variety of agents reflect the ability of the code to accurately treat both the complex fluid dynamic stabilization process as well as the chemical kinetics of the inhibited flame, and provide confidence in the numerically calculated flame structure to be discussed below.

Table 1. Experimental and numerical extinguishment limit and % error between them, oxidizer heat capacity, and adiabatic flame temperature for cup-burner flames at extinguishment.

Agent	$X_{a,\text{exp}}$	$X_{a,\text{cal}}$	$\frac{(X_{a,\text{cal}} - X_{a,\text{exp}})}{X_{a,\text{exp}}}$	$C_{p,\text{ox}}$ at $X_{a,\text{exp}}$ (J/mol K)	T_f (K) at $X_{a,\text{exp}}$
Br_2	0.0154 ± 0.001	0.0167	0.084	29.28	2186
CF_3Br	0.024 ± 0.001	0.0249	0.037	30.14	2174
CF_3H	0.117 ± 0.008	0.101	-0.137	31.74	2109
CO_2	0.157 ± 0.006	0.145	-0.076	30.43	1927
He	0.267 ± 0.011	0.222	-0.169	26.94	2001
N_2	0.259 ± 0.01	0.252	-0.027	29.16	1900
Ar	0.373 ± 0.015	0.357	-0.043	26.05	1875

4.2. FLAME STRUCTURE OF INHIBITED AND UNINHIBITED FLAMES

The structure of the uninhibited methane-air cup-burner flame in normal gravity has been described previously [32, 43]. The flames are laminar and nearly axisymmetric. The low fuel and air velocities used in the present investigation yield a weakly strained stable flame that is attached to the burner lip. The heat release in the flame, together with the low flow velocities promotes buoyancy-induced instabilities outside the flame surface causing it to flicker at a low frequency, as described previously [44]. The computed flame is oscillating at a low frequency with large toroidal vortices forming naturally outside the flame surface. The frequency corresponding to the passage of these vortices (also known as the flame-flickering frequency) is ~ 11 Hz, which compares well with the value measured in the experiments (10 to 15 Hz, according to the co-flow oxidizer velocity [44]).

For flames with added CF_3Br or Br_2 , the inhibitor is added to the air flow while reducing the air by a corresponding amount, so that the velocity is maintained constant. As CF_3Br is added, the flame base lifts off of the burner rim and moves inward. At a specific CF_3Br volume

fraction, the flame base detaches from the burner, drifts downstream and does not re-attach. (The behavior for Br_2 is similar.) For CF_3Br , Figure 1 shows the measured flame base height and radial position for the left and right halves of the flame, as well as that predicted by the numerical calculations. In both the experiment and the calculation, the location oscillates due to buoyancy induced flame flicker, and the error bars on the experimental points in **Error! Reference source not found.** show one standard deviation in the base location. As shown, the flame base height starts at about 0.5 mm with 0 % CF_3Br , decreases slightly for addition of 1 % CF_3Br , and then between 1.5 % and 2.0 % CF_3Br , lifts to about 2 mm. The flame radial position also starts to change at a CF_3Br loading of about 1 % to 1.5 %, at which it moves radially inward by about 2.5 mm. The magnitude of the base oscillation is relatively small up to 1 % CF_3Br , but above this value, it is about four times larger. The large solid squares in Figure 1 show the predicted flame base height and radius. As shown, the numerical prediction is in reasonable agreement with the experiments. The calculated reaction kernel height is about 30 % higher for Br_2 than for CF_3Br .

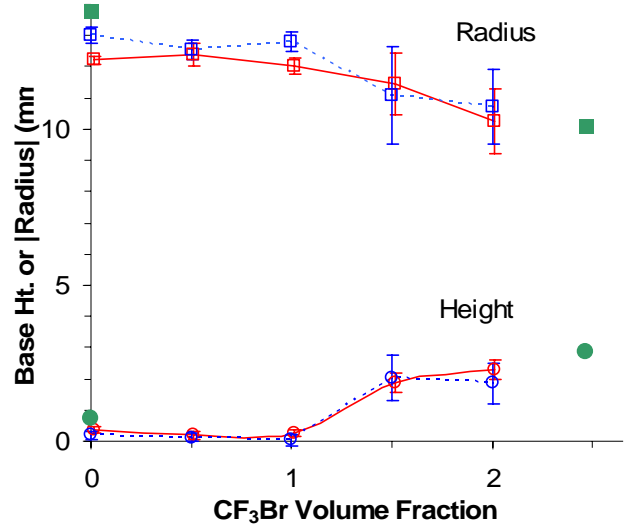


Figure 1 – Measured and calculated flame base radius and height for left (dotted) and right (solid) image of flame base with added CF_3Br . The larger solid green points at 0 % and 2.5 % CF_3Br are the model prediction.

The flame structure is shown in some detail in Figure 2 at one instant in the flickering cycle at which the vortex has convected away from the burner and is less influential. An uninhibited flame is shown in the top frame, while flames with $X_{\text{CF}_3\text{Br}} = 0.0246$ and $X_{\text{Br}_2} = 0.166$ (i.e., close to extinguishment) are shown in the middle and bottom frames, respectively. The variables include, on the right half: velocity vectors (\mathbf{v}), isotherms (T), total heat-release rate (\dot{q}), and the local equivalence ratio (ϕ_{local}); and on the left half: the total molar flux vectors of atomic hydrogen (\mathbf{M}_H), oxygen mole fraction (X_{O_2}), oxygen consumption rate ($-\hat{\omega}_{\text{O}_2}$), and mixture fraction (ξ), including stoichiometry ($\xi_{\text{st}} = 0.055$). The local equivalence ratio is defined [45] by considering a stoichiometric expression for intermediate species in the mixture to be converted to CO_2 and H_2O and is identical to the conventional equivalence ratio in the unburned fuel-air mixture. The mixture fraction was determined by the element mass fractions of carbon, hydrogen, and oxygen as defined by Bilger [46].

In Figure 2, the common features for the uninhibited flame (top) and the inhibited flames near lift-off (middle and bottom) are as follows. The velocity vectors show the longitudinal acceleration in the hot zone due to buoyancy, and as a result of the continuity of the fluid, surrounding air is entrained into the lower part of the flame, inclining the flow streamlines inward due to the low velocity of the fuel flow and the downstream acceleration. Both the heat-release rate and the oxygen-consumption rate contours show a peak reactivity spot (i.e., the

reaction kernel [30, 45, 47]) at the flame base, where the oxygen-rich entrainment flow crosses the flame zone, thus enhancing convective (and diffusive) contributions to the oxygen flux. On the other hand,

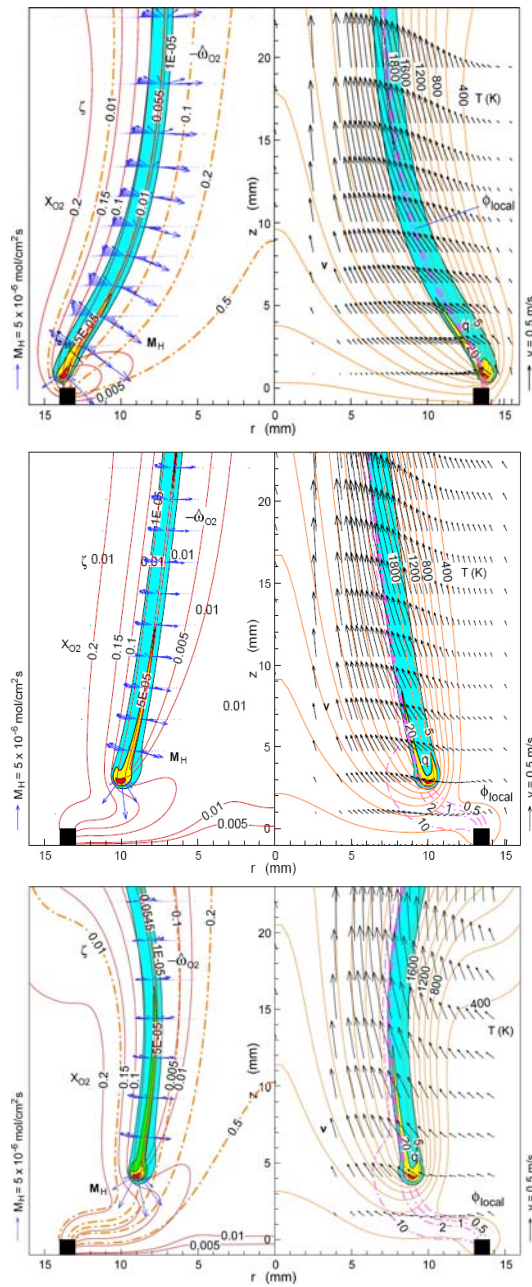


Figure 2 - Calculated structure of methane flames with no agent (top), 2.46 % CF_3Br (middle) or 1.66 % Br_2 (bottom), showing: (right half) velocity vectors, temperature, local equivalence ratio, heat release rate; (left half) X_{O_2} , H-atom flux vectors, $-\hat{\omega}_{\text{O}_2}$, mixture fraction. (\dot{q} contours: 5, 20, and 80 $\text{J}/\text{cm}^3\text{s}$; $-\hat{\omega}_{\text{O}_2}$ contours: 1×10^{-5} , 5×10^{-5} , and 2×10^{-4} $\text{mol}/\text{cm}^3\text{s}$).

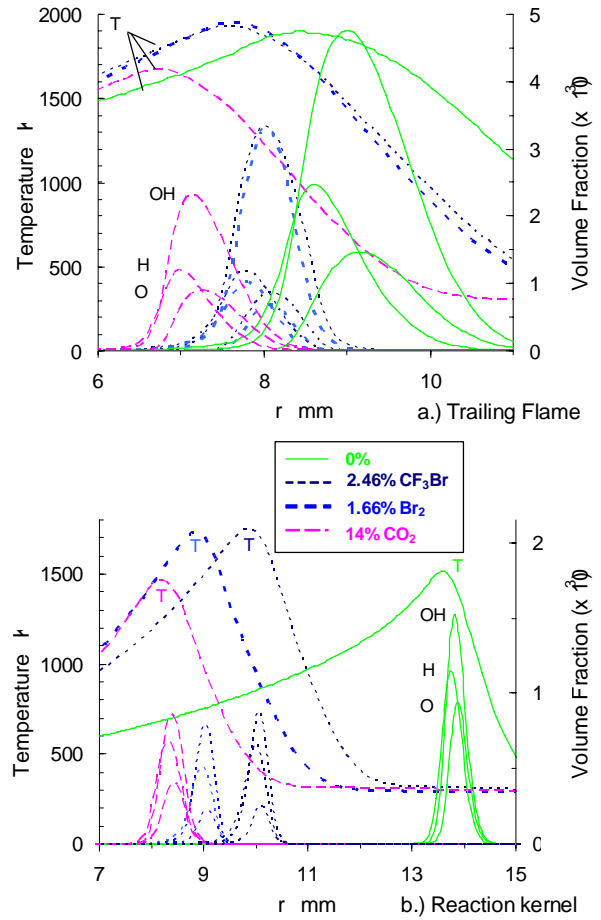


Figure 3 – Flame structures in (a) trailing diffusion flame (top), and (b) reaction kernel (bottom) regions of a cup-burner flame with 0 % and 2.46 % CF_3Br , 1.66 % Br_2 , or 14 % CO_2 added to the airflow.

chain radical species, particularly the H atom, diffuse back against the oxygen-rich incoming flow at the flame base (edge). As a result, chain-branching ($\text{H} + \text{O}_2 \rightarrow \text{OH} + \text{O}$) and subsequent exothermic reactions are enhanced particularly at the flame base, thus forming the reaction kernel. In the near-field region shown in Figure 2, except in the base ($z < 6$ mm) and tip regions, the temperature of the main reaction zone (i.e., the trailing diffusion flame) is 1880 K to 1900 K in the uninhibited flame and 1915 K to 1930 K with CF_3Br , and 1920 K to 1970 K with Br_2 . For the flames in Figure 2, Table 2 lists the heat-release rate, oxygen consumption rate, velocity, temperature, oxygen mole fraction, local equivalence ratio, and mixture fraction at the reaction kernel. Most of the properties for CF_3Br and Br_2 are similar, and these are also similar to those of the uninhibited flame, highlighting the dynamic nature of the reaction kernel, that seeks a location providing a balance between the flow velocity and the reaction rate. It is notable that the temperature at the reaction kernel in the flame inhibited by CF_3Br is 191 K higher than that in the uninhibited flame, whereas the heat-release rate is 18 % lower; for Br_2 , the temperature in the reaction kernel is 200 K higher and the heat release, 26 % lower.

Table 2. Reaction kernel properties.

Reaction kernel Property	Agent (i)		
	None	CF_3Br	Br_2
X_i	0	0.0246	0.0166
\dot{q}_k ($\text{J}\cdot\text{cm}^{-3}\cdot\text{s}^{-1}$)	155	127	115
$-\hat{\omega}_{\text{O}_2,k}$ ($\text{mol}\cdot\text{cm}^{-3}\cdot\text{s}^{-1}$)	0.00041	0.00034	0.00031
$ \mathbf{v}_k $ ($\text{m}\cdot\text{s}^{-1}$)	0.275	0.260	0.332
T_k (K)	1505	1696	1705
$X_{\text{O}_2,k}$	0.041	0.041	0.044
ξ_k	0.052	0.044	0.044

4.3. CHEMICAL DESCRIPTION OF CUP-BURNER FLAME EXTINGUISHMENT WITH CF_3BR OR BR_2

The structure of the flame base (edge) has been found to be important for understanding the stability of a *jet* diffusion flame [30, 45] and of the extinguishment of cup-burner flames by CF_3H [33], and it is likely to be important for the present flames with brominated inhibitors as well. As described above, with 2.46 % CF_3Br , the reaction kernel is located at a height of 2.84 mm above the burner lip; for 1.67 % Br_2 , it is calculated to be at 4.04 mm. The structure of the flame is investigated in detail at this height, as well as in the trailing diffusion flame at a height 10 mm above the reaction kernel. Since radical concentrations are important for flame stability, Figure 3 shows the calculated temperature and radical volume fractions as a function of radial location in: (a.) top image, trailing diffusion flame, and (b.) bottom image, reaction kernel. Data are shown for uninhibited flames (solid lines), and those with $X_{\text{Br}_2}=0.0166$ (thick dotted lines) and $X_{\text{CF}_3\text{Br}} = 0.0246$ (thin dotted lines). For comparison, results are also shown for addition of a physically acting agent (CO_2 , dashed lines) near the extinguishment limit, $X_{\text{CO}_2}=0.14$, (from [44], Fig. 6, at an elapse time of 0.08 s from the flame-base detachment).

In the trailing diffusion flame (top frame), the most striking features are that the properties for CF₃Br or Br₂ addition are very similar, and the net effect from CO₂ addition on the radicals is also similar (although the reduction is achieved in a different way). For example, without inhibitor, the peak temperature in the trailing diffusion flame is 1900 K, and the peak volume fractions of OH, H, and O are 0.0047, 0.0024, and 0.0015. Addition of CO₂ lowers the peak temperature to 1674 K, whereas addition of CF₃Br raises it to 1930 K (due to the additional heat release per unit mass of oxidizer from CF₃Br reaction), and addition of Br₂ raises it even more, to 1970 K (due to the higher effective oxidizer volume fraction in the oxidizer stream, since Br₂ is additional oxidizer). Radical volume fractions are reduced comparably with addition of any of the agents: peak [H] and [O] are reduced by about 50 % with each of the agents, as is [OH] with CO₂ addition, whereas CF₃Br or Br₂ addition reduces [OH] by only 30 %. In all cases, the radical volume fractions peak on the air side of the temperature peak, especially for OH, and O (due to the usual inhibiting effect of the hydrocarbon species on the chain branching reactions).

At the height across the reaction kernel, the effect of the additives on the radicals is again similar, although the reaction kernel location is slightly different. The peak temperatures are significantly lower than in the trailing diffusion flame, 1517 K, 1465 K, 1749 K, 1730 K, for the uninhibited, CO₂, CF₃Br, and Br₂ flames. In the uninhibited flame, the peak radical volume fractions of OH, H, and O in the reaction kernel are 0.0015, 0.0011, and 0.00095, so that compared with the trailing diffusion flame (height of 10 mm downstream of the reaction kernel), [OH] is about a factor of three lower, [H], about a factor of two lower, and [O], about the same. Adding the inert agent CO₂ (or similar inert agents [48]) lowers the temperature in the reaction kernel only mildly, 52 K (since the reaction kernel moves so as to balance the local reaction rate with the local flow field), as compared to a 232 K decrease in the temperature in the trailing flame. On the other hand, addition of CF₃Br *raises* the reaction kernel temperature by 232 K (and Br₂ by 213 K), as compared to a 30 K (50 K for Br₂) increase in the temperature in the trailing flame. Nonetheless, radical volume fractions are still reduced in the reaction kernel, although to a slightly smaller degree than in the trailing diffusion flame. For example, [OH] and [H] are reduced about 41 % with CO₂, CF₃Br, or Br₂ addition, while [O] is reduced about 55 % with CO₂ addition or 72 % with CF₃Br or Br₂ addition. As in the trailing diffusion flame, addition of CF₃Br or Br₂ has a very similar effect on the radical volume fractions.

Figure 4 shows the structure of the uninhibited flames (left), or those with X_{CF₃Br}=0.0246 (middle), or X_{Br₂}=0.0166 (right) in the trailing flame (top) or reaction kernel (bottom) region. In all frames (left scale), the reaction flux (i.e., the sum of the local reaction rates in mol/cm³/s) is given for the sum of all hydrocarbon reactions (HC) involving OH, H, and O for the production (+) and consumption (-) of these chain-carrying radicals, as well as the net effect from hydrocarbon reactions (HC_{net}). Also shown are corresponding sums for reactions involving halogenated species (F⁺, F⁻, and F_{net}), and the sum of both the hydrocarbon and halogen reactions involving those radicals (Net_{net}). In all frames (the right scale), the radial profiles of temperature (T, K), heat release rate (Q, J/cm³/s), and volume fraction (x 10⁷) of CH₄, O₂, and inhibitor (CF₃Br or Br₂) are also provided.

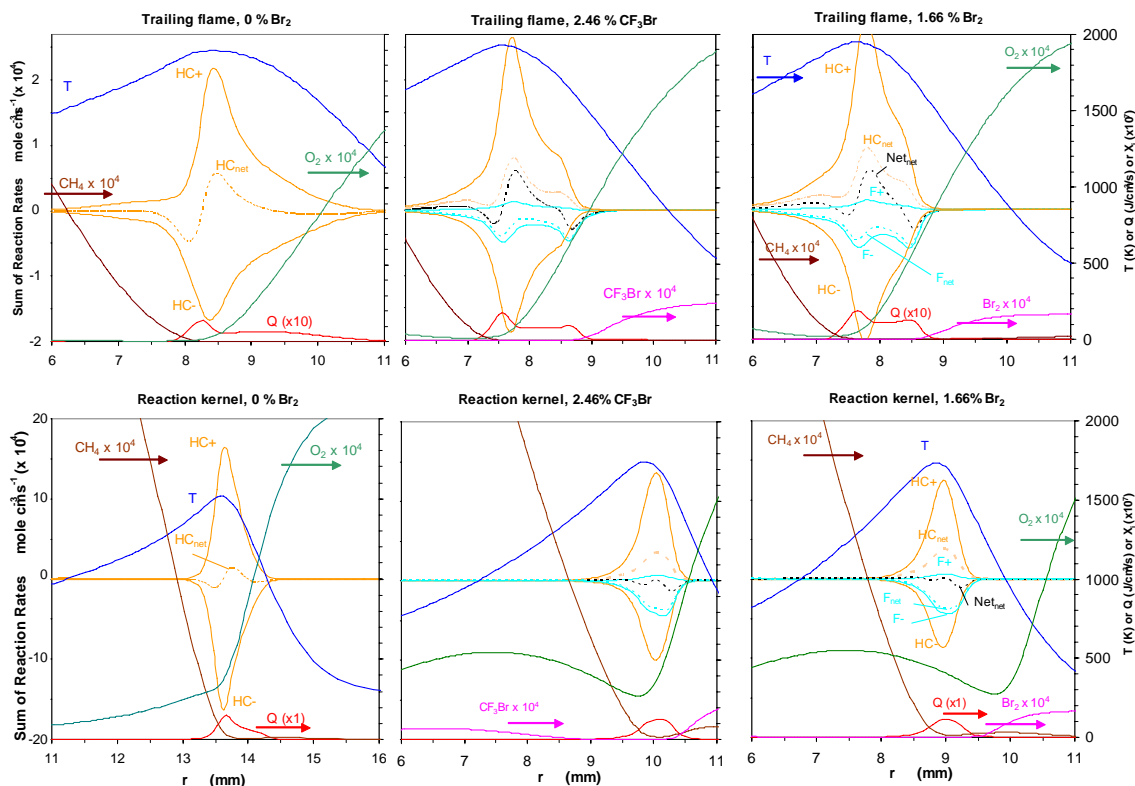


Figure 4 – Sum of reaction rates (left scale) of all reactions involving H, O, or OH, for CH₄-air cup-burner flame with no agent (left), 2.46 % CF₃Br (middle) or 1.66 % Br₂ (right). The top frames: trailing diffusion flame; bottom: reaction kernel. Curves are shown for production (+), consumption (-) and the summed (net) effect on radical fluxes, for the halogen (F) and hydrocarbon (HC) reactions. Also shown (using the right scale) are the temperature and heat release, as well as the species volume fraction for O₂, CH₄, and CF₃Br or Br₂ (curve labels in the middle frames are the same as the right frames unless otherwise marked).

In the trailing region of the flame (top frames), the major species volume fractions for the uninhibited case (left frame) are those in a typical diffusion flame [ref??]. For example, in the top left graph of Figure 4, the CH₄ and O₂ are shown to be consumed at a radial location near, but slightly interior to, that of the peak temperature and peak heat release rate. For the inhibited flames (middle and right, top) the CH₄ and O₂ are again consumed slightly interior to the peak temperature, but heat release occurs throughout the region of radical production.

In the reaction kernel (bottom frames of Figure 4), the flames have a partially premixed character. There is significant penetration of the oxidizer into the fuel stream, even for the uninhibited flame. With addition of CF₃Br, the flame lifts significantly, allowing oxygen levels at the radial location of the branching reactions to reach 3 to 4 times higher than in the trailing part of the flame. The lifted flame also allows the CF₃Br to penetrate into the fuel stream.

The radial distribution of heat release rate is also shown in Figure 4. For both uninhibited and CF₃Br- or Br₂-inhibited flames, the peak heat release rate in the trailing flame is about ten times lower, and has a broader distribution than in the reaction kernel. The heat release rate generally

scales with the reaction flux for the radicals (as shown in Figure 3) for all conditions shown. It is interesting to note that in the trailing diffusion flame, the peak heat release rate per unit volume is about 30 % higher with CF_3Br or Br_2 than without; whereas, in the reaction kernel (where flame destabilization actually occurs), addition of CF_3Br or Br_2 lowers the peak heat release per unit volume, but only by about 15 %.

The effect of CF_3Br on the radicals can be seen through examination of their reaction fluxes. For the trailing region of the uninhibited flames (top left), the hydrocarbon reactions are net producers of radicals on the oxidizer side of the flame, but net consumers of radicals on the fuel side. With addition of either CF_3Br or Br_2 (top, middle or right), the hydrocarbon reactions are everywhere net producers of radicals, while the reactions with halogen species are everywhere net consumers. For the sum of all reactions (Net_{net}), the production of radicals is limited to the central portion of the reaction zone, where mole fractions of *both* the fuel and the inhibitor are low, while the net consumption occurs near the edges of this region, highlighting the effect of CF_3Br or Br_2 themselves on the radicals.

For the reaction kernel, Figure 4 (lower frames) shows that the magnitude of the reaction fluxes (both production and consumption) for radicals is 5 to 8 times higher than in the trailing diffusion flame, despite the lower temperature there (note the scale change on the left ordinate). In the reaction kernel, the radical volume fractions are a few times lower than in the trailing diffusion flame, but they are both produced and consumed at a much higher rate. As discussed previously for other agents [48], this is due to the high rate of chain branching facilitated by the high volume fraction of O_2 from the mixing underneath the lifted base region. The effect of the brominated species on the radical pool in the reaction kernel (lower, middle and right frames) is again indicated by the reaction fluxes, where reactions with the halogenated species (F_{net}) consume radicals which are produced by reactions with the hydrocarbon species (HC_{net}). The net effect of all reactions in the region (Net_{net} , from reaction with both hydrocarbon and halogen-containing species), however, is a net consumption of radicals. Hence, they must be supplied by diffusion from upper regions (i.e., the trailing diffusion flame), as also indicated in Figure 2 (bottom left), which shows the high flux of H atoms at the reaction kernel. Since reactions of halogen-containing species with radicals play a key role in weakening the flame base, it is of interest to examine which reactions are responsible.

Figure 5 shows the reaction flux by radical reaction with halogenated species in more detail. The net reaction flux of chain-carrying radicals (symmetrical about zero flux) is shown by the left scale, while the reaction fluxes for the regeneration steps of HBr from Br is given by the right axis (up from zero). The reaction kernel case (bottom graph) is simpler. For CF_3Br addition, about 95 % of the radical consumption by reaction with halogenated species is due to HBr reaction with H or OH (H more important than with OH), and most of the remainder is due to Br_2 reaction with H; with Br_2 addition, nearly all of the radical consumption is due to these reactions. Thus, for CF_3Br addition, the net contribution to the total halogen radical consumption by the fluorinated species is only about 10 % (in the reaction kernel).

In the trailing diffusion flame with CF_3Br addition (top, left frame), the importance of the bromine reactions to the radical reduction is even stronger. Although not shown in the figure for clarity, one can construct a reaction flux curve for the sum of Br-containing reactions which

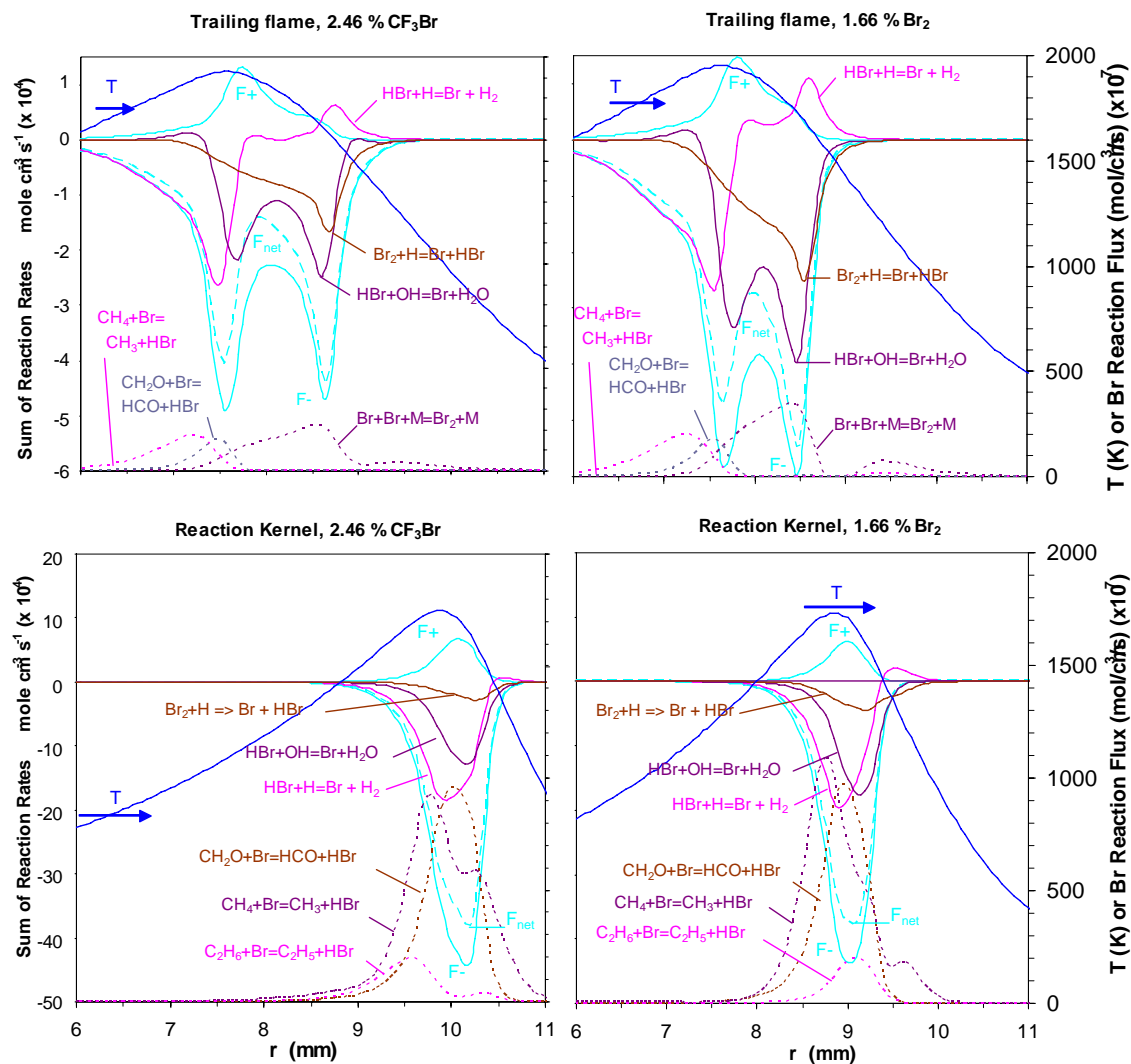
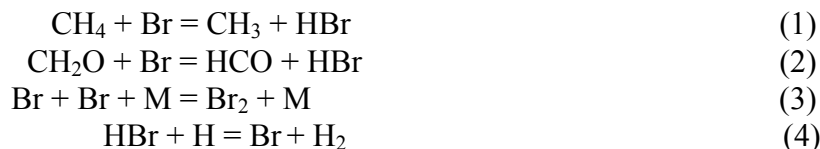


Figure 5 – Detail from Figure 4 of sum of reaction rates for all reactions involving H, O, or OH, with addition of 2.46 % CF₃Br (left frames) or 1.66 % Br₂ (right frames); top figure: trailing diffusion flame, bottom figure: reaction kernel. For radical consumption, the total is shown for all halogen reactions (F-), as well as the contribution from radical reaction with specific reactions of HBr or Br₂. In both flames (top and bottom frames), the important reactions reforming HBr and Br₂ are also shown (dotted lines, right scale).

recombine radicals. That curve is *greater* in magnitude than the net consumption by the sum of all halogenated reactions (F_{net}); that is, in the trailing diffusion flame, reactions with fluorinated species (as well as those with hydrocarbon species) are net *producers* of radicals, and hence *all* of the consumption comes from reactions with brominated species. In the trailing diffusion flame, $\text{HBr} + \text{OH}$ is the most important radical recombining reaction, followed by $\text{Br}_2 + \text{H}$; interestingly, the $\text{HBr} + \text{H}$ reaction is a net consumer of chain-carrying radicals on the fuel side, but a net producer of them on the oxidizer side of the flame, highlighting the reversible nature of the catalytic cycle.

In the trailing flame (Figure 5 top frames), there is a large depression in the radical consumption flux curve at a radial position near 8 mm, for either CF_3Br or Br_2 addition. To investigate this, we have plotted the reaction rates for the reactions which regenerate the species (HBr and Br_2) necessary for the inhibition cycle. For CF_3Br addition, these reactions,



are shown (top, left frame) to occur in regions which exclude the central portion of the radical consumption region: the first two reactions need hydrocarbon fragments, which are present only at the fuel side, and the third reaction needs Br and is favored at lower temperatures, which cause it to be favored on the oxidizer side. The final reaction is only a source of HBr as the temperature decreases on the air side of the peak T , and the equilibrium for reaction (4) shifts to the left. The results with Br_2 addition are similar. In contrast, in the reaction kernel (Figure 5 bottom frames), the most important reactions for catalytic species regeneration overlap with the radical location much more effectively than they do in the trailing diffusion flame, and their rates are about twice as fast. Hence, in the reaction kernel, due to good upstream mixing, the effectiveness of the bromine catalytic cycles is not as limited by the regeneration steps as it is in the trailing diffusion flame. This highlights the suggestion [49] that a key element in a catalytic cycle is the regeneration of the catalytic intermediates. These results are consistent with the finding [50] that the relative performance advantage of CF_3Br over CO_2 depends upon the flame type, with a lower advantage in counterflow diffusion flames relative to premixed flames. Note that due to the premixing in the reaction kernel where stabilization takes place, cup-burner flame extinguishment is more similar to premixed flame propagation than counterflow diffusion flame extinction, as has been discussed previously [48].

A result of the more effective inhibition in the reaction kernel is that the flame will always be destabilized first at the base (observed in both the calculations and the experiment). This occurs since the catalytic cycles are more effective there, and because the reaction kernel depends upon the downstream flame (which has higher radical volume fractions) as a source of radicals via diffusion.

6. CONCLUSIONS:

Cup-burner flames of methane and air with added CF_3Br or Br_2 have been studied experimentally and numerically. The numerical code has predicted the flame extinguishment volume fraction within about 4 % of experiment value for pure CF_3Br , and 8 % for Br_2 . The flame base lift-off has been predicted for CF_3Br within the experimental error. The flame is extinguished by a blow-off process rather than global extinction. With CF_3Br added at near-extinguishing conditions, the flame temperature is higher everywhere as compared to the uninhibited flame, so that any increases in the average heat capacity of the oxidizer is more than offset by heat release from inhibitor reaction.

The chemical details of cup-burner flame extinguishment by CF_3Br or Br_2 are strikingly similar. At near-extinguishing CF_3Br or Br_2 volume fraction (0.0246 or 0.0167), the cup-burner flame is characterized by two regions: the reaction kernel, which is responsible for stabilizing the flame at the base, and the trailing diffusion flame, which serves as a source of radicals for the reaction kernel. While the volume fraction of chain-carrying radicals (O, H, and OH) is lower in the reaction kernel, the reaction flux of radicals there is a factor of five higher, and the heat release rate is also higher (by a factor of ten). CF_3Br or Br_2 serves to reduce the radical volume fraction in both regions, although the mechanism differs somewhat. In the reaction kernel, radicals are consumed primarily through a catalytic cycle involving HBr reaction with H or OH, with small additional contribution from the CF_3 fragment. In the trailing diffusion flame, the recombination of radicals is solely due to bromine catalytic cycles, with reactions with fluorinated fragments serving to produce radicals somewhat. In this downstream region of the flame, effective radical recombination is limited by the regeneration steps for HBr in the catalytic cycle which depend upon hydrocarbon species, that are scarce at the flame zone (where the peak radical volume fraction is located). As a result, the less efficient catalytic cycle in the trailing diffusion flame reduces the radical volume fractions there somewhat less as compared to the reaction kernel.

7. ACKNOWLEDGMENTS:

This work was supported by the Office of Biological and Physical Research, NASA, Washington, D. C.

8. REFERENCES:

1. Gann, R. G. *Halogenated Fire Suppressants*, ACS Symposium Series 16, American Chemical Society, Washington, DC, 1975.
2. Andersen, S. O., "Halon and the Stratospheric Ozone Issue," *Fire Journal*, **81**, 56, 1987.
3. Morrisette, P. M., "The Evolution of Policy Responses to Stratospheric Ozone Depletion," *Natural Resources Journal*, **29**, 793, 1989.
4. Grosshandler, W. L., Gann, R. G., and Pitts, W. M., "Evaluation of Alternative In-Flight Fire Suppressants for Full-Scale Testing in Simulated Aircraft Engine Nacelles and Dry Bays", NIST SP 861, 1994.
5. Gann, R. G., "Fire Suppression System Performance of Alternative Agents in Aircraft Engines and Dry Bay Laboratory Simulations", NIST SP 890, vols. I and II, 1995.

6. Gann, R. G., "FY2003 Annual Report -- Next Generation Fire Suppression Technology Program (NGP)", National Institute of Standards and Technology, NIST Technical Note 1457, 2004.
7. Casias, C. R. and McKinnon, J. T., "A Modeling Study of the Mechanisms of Flame Inhibition by CF_3Br Fire Suppressant Agent," *Proc. Combust. Inst.*, **27**, 2731, 1998.
8. Vora, N. and Laurendeau, N. M., "Analysis of CF_3Br Flame Suppression Activity Using Quantitative Laser-Induced Fluorescence Measurements of the Hydroxyl Radical," *Combust. Sci. Technol.*, **166**, 15, 2001.
9. Kim, C. H., Kwon, O. C., and Faeth, G. M., "Effects of Halons and Halon Replacements on Hydrogen-Fueled Laminar Premixed Flames," *J. Propul. Power*, **18**, 1059, 2002.
10. Saso, Y., "Roles of Inhibitors in Global Gas-Phase Combustion Kinetics," *Proc. Combust. Inst.*, **29**, 337, 2003.
11. Williams, B. A. and Fleming, J. W., " CF_3Br and Other Suppressants: Differences in Effects on Flame Structure," *Proc. Combust. Inst.*, **29**, 345, 2003.
12. Bundy, M., Hamins, A., and Lee, K. Y., "Suppression Limits of Low Strain Rate Non-Premixed Methane Flames," *Combust. Flame*, **133**, 299, 2003.
13. Seshadri, K., "Chemical Inhibition of Nonpremixed Methane Flames by CF_3Br ," *Combust. Sci. Technol.*, **177**, 871, 2005.
14. Bajpai, S. N., "An Investigation of the Extinction of Diffusion Flames by Halons," *Journal of Fire and Flammability*, **5**, 255, 1974.
15. Hirst, B. and Booth, K., "Measurement of Flame Extinguishing Concentrations," *Fire Technol.*, **13**, 296, 1977.
16. NFPA, "Clean Agents Fire Extinguishing Systems", 2001, 1999.
17. Anon, "Gaseous Fire-Extinguishing Systems Physical Properties and System Design", ISO 14520-Part I, 2000.
18. Simmons, R. F. and Wolfhard, H. G., "The Influence of Methyl Bromide on Flames, Part 2.- Diffusion Flames," *Trans. Faraday Soc.*, **52**, 53, 1956.
19. Sheinson, R. S., Pender-Hahn, J. E., and Indritz, D., "The Physical and Chemical Action of Fire Suppressants," *Fire Safety Journal*, **15**, 437, 1989.
20. Lott, J. L., Christian, S. D., Sliepcevich, C. M., and Tucker, E. E., "Synergism Between Chemical and Physical Fire-Suppressant Agents," *Fire Technol.*, **32**, 260, 1996.
21. Rosser, W. A., Wise, H., and Miller, J., "Mechanism of combustion inhibition by compounds containing halogen," *Proc. Combust. Inst.*, **7**, 175, 1959.
22. Butlin, R. N. and Simmons, R. F., "The inhibition of hydrogen-air flames by hydrogen bromide," *Combust. Flame*, **12**, 447, 1968.
23. Day, M. J., Stamp, D. V., Thompson, K., and Dixon-Lewis, G., "Inhibition of Hydrogen-Air and Hydrogen-Nitrous Oxide Flames by Halogen Compounds," *Proc. Combust. Inst.*, **13**, 705, 1971.
24. Dixon-Lewis, G. and Simpson, R. J., "Aspects of Flame Inhibition by Halogen Compounds," *Proc. Combust. Inst.*, **16**, 1111, 1977.
25. Westbrook, C. K., "Numerical Modeling of Flame Inhibition by CF_3Br ," *Combust. Sci. Technol.*, **34**, 201, 1983.
26. Westbrook, C. K., "Inhibition of Methane-Air and Methanol-Air Flames by HBr ," *Combust. Sci.*

- Technol.*, **23**, 191, 1980.
27. Westbrook, C. K., "Inhibition of Hydrocarbon Oxidation in Laminar Flames and Detonations by Halogenated Compounds," *Proc. Combust. Inst.*, **19**, 127, 1982.
 28. Noto, T., Babushok, V., Burgess Jr., D. R., Hamins, A., Tsang, W., and Miziolek, A., "Effect of Halogenated Flame Inhibitors on C1-C2 Organic Flames," *Proc. Combust. Inst.*, **26**, 1377, 1996.
 29. Takahashi, F. and Katta, V. R., "Attachment Mechanisms of Diffusion Flames," *Proc. Combust. Inst.*, **27**, 675, 1998.
 30. Takahashi, F. and Katta, V. R., "A Reaction Kernel Hypothesis for the Stability Limit of Methane Jet Diffusion Flames," *Proc. Combust. Inst.*, **28**, 2071, 2000.
 31. Takahashi, F. and Katta, V. R., "Reaction Kernel Structure and Stabilizing Mechanisms of Jet Diffusion Flames in Microgravity," *Proc. Combust. Inst.*, **29**, 2509, 2003.
 32. Takahashi, F., Linteris, G. T., and Katta, V. R., "Extinguishment Mechanisms of Cup-Burner Flames," *44th Aerospace Sciences Meeting and Exhibit*, AIAA, p. AIAA Paper No. 2006, 2006.
 33. Katta, V. R., Takahashi, F., and Linteris, G. T., "Fire-suppression characteristics of CF₃H in a cup burner," *Combust. Flame*, **144**, 645, 2006.
 34. Linteris, G. T. and Gmurczyk, G. W., "Fire Suppression System Performance of Alternative Agents in Aircraft Engine and Dry Bay Laboratory Simulations", SP-890, vol. II, 1995.
 35. Walsh, K. T., Long, M. B., Tanoff, M. A., and Smooke, M. D., "Experimental and Computational Study of CH, CH*, and OH* in an Axisymmetric Laminar Diffusion Flame," *Proc. Combust. Inst.*, **27**, 615, 1998.
 36. Klimek, R. and Wright, T., "Spotlight 1.1," NASA Glenn Research Center, Cleveland, OH, <http://microgravity.grc.nasa.gov/spotlight/>, 2002.
 37. Roquemore, W. M. and Katta, V. R., "*Journal of Visualization*, **2**, 257, 2000.
 38. Burgess, D. R., Zachariah, M. R., and Tsang, W., "NIST WWW CKMech Mechanisms," <http://www.cstl.nist.gov/div836/ckmech/nisthfc.html>, 1999.
 39. Frenklach, M., Wang, H., Yu, C.-L., Goldenberg, M., Bowman, C. T., Hanson, R. K., Davidson, D. F., Chang, E. J., Smith, G. P., Golden, D. M., Gardiner, W. C., and Lissianski, V., "GRI-Mech: An Optimized Detailed Chemical Reaction Mechanism for Methane Combustion", Gas Research Institute Topical Report, No. GRI-95/0058, http://www.me.berkeley.edu/gri_mech, 1995.
 40. Anon, "Computational Submodels, International Workshop on Measurement and Computation of Turbulent Nonpremixed Flames," <http://www.ca.sandia.gov/tdf/Workshop/Submodels.html>, 2001.
 41. Katta, V. R., Takahashi, F., and Linteris, G. T., "Suppression of Cup-Burner Flames Using Carbon Dioxide in Microgravity," *Combust. Flame*, **137**, 506, 2004.
 42. Takahashi, F., Linteris, G. T., and Katta, V. R., "Flame Extinguishment in a Cup Burner Apparatus," *Fourth Joint Meeting of the U.S. Sections of The Combustion Institute, March 2005.*, 2005.
 43. Katta, V. R., Takahashi, F., and Linteris, G. T., "Numerical Investigations of CO₂ as Fire Suppressing Agent," *Fire Safety Science: Proc. of the Seventh Int. Symp.*, Int. Assoc. for Fire Safety Science, p. 531, 2003.
 44. Takahashi, F., Linteris, G. T., and Katta, V. R., "Vortex-Coupled Oscillations of Edge Diffusion Flames in Coflowing Air with Dilution," *Proc. Combust. Inst.*, **31**, in press., 2006.

45. Takahashi, F. and Katta, V. R., "Structure of Propagating Edge Diffusion Flames in Hydrocarbon Fuel Jets," *Proc. Combust. Inst.*, **30**, 375, 2005.
46. Bilger, R. W., "The Structure of Turbulent Non-Premixed Flames," *Proc. Combust. Inst.*, **22**, 1377, 1988.
47. Takahashi, F. and Katta, V. R., "Further Studies of the Reaction Kernel Structure and Stabilization of Jet Diffusion Flames," *Proc. Combust. Inst.*, **30**, 383, 2005.
48. Takahashi, F., Linteris, G. T., and Katta, V. R., "Extinguishment Mechanisms of Co-flow Diffusion Flames in a Cup-Burner Apparatus," *Proc. Combust. Inst.*, **31**, in press., 2006.
49. Babushok, V. , Tsang, W., Linteris, G. T., and Reinelt, D., "Chemical limits to flame inhibition," *Combust. Flame*, **115**, 551, 1998.
50. Takahashi, F., Linteris, G. T., and Katta, V. R., "Experimental and Numerical Evaluation of Gaseous Agents for suppression Cup-Burner Flames in Low Gravity," *7th International Workshop on Microgravity Combustion and Chemically reacting Systems*, NASA, p. 277, 2003.